

Elsevier Editorial System(tm) for Coastal
Engineering
Manuscript Draft

Manuscript Number: CENG-D-16-00062R1

Title: Correcting Wave Reflection Estimates in the Coastal Zone

Article Type: Research Paper

Keywords: Wave reflection; noise; coherence; linear wave theory

Corresponding Author: Mr. Kris Inch,

Corresponding Author's Institution: University of Plymouth

First Author: Kris Inch

Order of Authors: Kris Inch; Mark Davidson; Gerd Masselink; Paul Russell

Abstract: The impact of random noise on an existing two-dimensional method for separating incident and reflected wave spectra using an array of wave gauges is investigated using simulated time series with known wave amplitudes, reflection coefficients, and signal-to-noise ratios. Both the incident and reflected spectra are overestimated by a quantity that can exceed 100% for signal-to-noise ratios less than 1. Consequently, estimated reflection coefficients are also overestimated with larger errors occurring when the known reflection is low. Coherence decreases systematically with increasing noise and this trend is used to develop a mathematical function to correct for the observed bias and provide 95% confidence intervals for incident and reflected spectra and reflection coefficients. The correction technique is shown to be very effective in reducing error by up to ~90%. Field data from a natural beach are used to demonstrate the application of these results; corrected values suggest that reflection coefficients are frequently overestimated by over 50%.

Correcting Wave Reflection Estimates in the Coastal Zone

Kris Inch^{*}, Mark Davidson, Gerd Masselink and Paul Russell

*School of Marine Science and Engineering, Plymouth University, Drake Circus, Plymouth,
Devon PL4 8AA. United Kingdom. kris.inch@plymouth.ac.uk, M.Davidson@plymouth.ac.uk,
gerd.masselink@plymouth.ac.uk, P.Russell@plymouth.ac.uk*

* Corresponding author. Tel.: +44 (0)1752 586100; Fax: +44 (0)1752 586101; Email:
kris.inch@plymouth.ac.uk (Kris Inch).

Abstract

The impact of random noise on an existing two-dimensional method for separating incident and reflected wave spectra using an array of wave gauges is investigated using simulated time series with known wave amplitudes, reflection coefficients, and signal-to-noise ratios. Both the incident and reflected spectra are overestimated by a quantity that can exceed 100% for signal-to-noise ratios less than 1. Consequently, estimated reflection coefficients are also overestimated with larger errors occurring when the known reflection is low. Coherence decreases systematically with increasing noise and this trend is used to develop a mathematical function to correct for the observed bias and provide 95% confidence intervals for incident and reflected spectra and reflection coefficients. The correction technique is shown to be very effective in reducing error by up to ~90%. Field data from a natural beach are used to demonstrate the application of these results; corrected values suggest that reflection coefficients are frequently overestimated by over 50%.

Keywords: *Wave reflection, noise, coherence, linear wave theory.*

1. Introduction

Wave reflection is an important process influencing the hydro- and sediment dynamics in front of natural coastlines and man-made coastal structures. Therefore, understanding and accurately predicting the magnitude of wave reflection is essential for estimating potential storm damage, modelling shoreline change, and assessing the reflection performance of marine structures.

Several methods exist to decompose a two-dimensional wave signal propagating over a horizontal bed into its incident and reflected components using cross-shore arrays of spatially separated wave gauges. These methods utilise the phase difference between pairs of wave gauges to provide information on the propagation of the incident and reflected waves. Early methods to calculate wave reflection typically use an array of only two wave gauges (e.g., Goda and Suzuki, 1976; Morden et al., 1976); however, these techniques suffer from singularities at a discrete number of critical frequencies where the distance between the two wave gauges is equal to an integer number of half the corresponding wavelength. To overcome this limitation and estimate wave reflection over a wider frequency range, several newer techniques have been developed that use the wave records from three or more wave gauges (e.g., Battjes et al., 2004; Gaillard et al., 1980; Mansard and Funke, 1980), thus providing a range of wave gauge pairs and separation distances for use in the analysis.

An alternative method of calculating wave reflection is to use a co-located wave gauge and velocity sensor (e.g., Guza and Bowen, 1976; Sheremet et al., 2002), where the direction of wave propagation is estimated using information on the slope of the sea surface provided by

1 the cross-shore current. These methods have the advantage of estimating wave reflection at a
2 singular cross-shore location, whereas the wave reflection estimate from an array method is
3 the average value for the spatial extent of the array, which may be quite large. Additionally,
4 methods that use a co-located wave gauge and velocity sensor are not affected by variations
5 in the bathymetry. However, it is critically important to have the wave gauge and velocity
6 sensor located at the same horizontal location as even a small spatial separation can have
7 important effects on the resulting wave reflection estimates (Huntley et al., 1999). In many
8 cases array methods remain the preferred approach as wave gauges are typically less intrusive
9 to deploy in the field than current sensors and far more economical if wave reflection
10 estimates are required at several cross-shore locations (Hughes, 1993).

26 Most array methods used to separate incident and reflected waves are designed for two-
27 dimensional waves propagating over a horizontal bed and do not account for the effects of
28 sloping bathymetry such as that of a natural beach. Therefore, depending on the wave
29 conditions and bed slope, errors in the analysis are likely when used in such conditions.

36 Baldock and Simmonds (1999) demonstrated that relatively simple modifications are required
37 to adapt the separation method of Frigaard and Brorsen (1995) to account for shore-normal
38 linear waves propagating over a bed with arbitrary bathymetry. Their analysis showed that
39 neglecting the shoaling effects of waves can lead to large errors in the estimated reflection
40 coefficient (the ratio of reflected to incident wave energy) in cases of low wave reflection.

48 Furthermore, accounting for bathymetry variations was found to be crucial to avoid
49 significant errors (up to 90%) in estimating the incident and reflected wave amplitudes.

56 An additional source of error that may impact wave reflection estimates, present in both
57 laboratory and field data, is that of noise. Potential sources of signal noise include water

1 surface variability that is unrelated to wave motion, proximity to standing wave nodes, and
2 electronic noise. Using simulated time series of surface elevation and velocity with known
3 true reflection coefficients and added uncorrelated noise, Huntley et al. (1999) show that the
4 presence of noise in the data can introduce a significant positive bias to the reflection
5 coefficients estimated from co-located wave gauge and velocity sensor methods. In an
6 attempt to overcome this, Tatavarti et al. (1988) developed a method using principal
7 component analysis to separate the elevation and velocity time series into orthogonal
8 eigenvector combinations, thus allowing the *correlated* parts of the two time series to be
9 separated from undesired noise. This technique was validated by Huntley et al. (1999) who
10 also demonstrate that the bias in reflection coefficients estimated using other co-located wave
11 gauge and velocity sensor methods can be corrected for by using the estimated reflection
12 coefficient itself and the coherence between the estimated incident and reflected waves. A
13 similar investigation into the effect of noise on wave reflection estimates using array methods
14 is currently lacking.

15
16
17
18
19
20
21
22
23
24
25
26
27
28
29
30
31
32
33
34
35
36 The aim of this paper is to use simulated time series of water surface elevation to investigate
37 the impact of noise on wave reflection estimates using the array method of Gaillard et al.
38 (1980). A mathematical function is developed to provide a correction for the observed bias in
39 incident and reflected spectra and corresponding reflection coefficients. This function is
40 applied to field data to demonstrate its value. The results presented in this paper are
41 principally applicable to the array method of Gaillard et al. (1980) which was chosen for its
42 relatively simple approach that directly returns incident and reflected spectra from which to
43 assess the noise impact. However, the procedure outlined in the following section could
44 equally be used to assess the impact of noise on other two-dimensional array methods.

2. Methodology

The water surface elevation η at two cross-shore locations, x_1 and x_2 , separated by Δx , is given by linear wave theory as

$$\eta(x_1, t) = a_i \cos(\omega t - kx_1 + \phi_i) + a_r \cos(\omega t + kx_1 + \phi_r) \quad (1)$$

$$\eta(x_2, t) = a_i \cos(\omega t - kx_1 - k\Delta x + \phi_i) + a_r \cos(\omega t + kx_1 + k\Delta x + \phi_r) \quad (2)$$

where t is time, a is wave amplitude, ω is wave angular frequency ($2\pi f$, where f is frequency), k is wavenumber ($2\pi/L$, where L is wavelength), ϕ is phase, and subscript i and r denote incident and reflected waves, respectively. The signs of the terms are for an onshore-directed x -axis. Eqs. (1) and (2) show that between cross-shore locations x_1 and x_2 , the incident and reflected waves are phase shifted by $-k\Delta x$ and $k\Delta x$, respectively. Eqs. (1) and (2) are used to generate simultaneous time series of water surface elevation at three cross-shore locations on a horizontal bed.

For the purpose of the simulations, wave amplitudes a_i and a_r are independent of frequency and all waves travel at the shallow water wave speed. A range of simulations were performed with incident wave amplitudes between 1 and 10 m, known reflection coefficients between 0 and 1, and with normally distributed, random noise added to the time series at known signal-to-noise ratios (SNR). While the use of constant wave amplitudes and reflection coefficients across all frequencies is not representative of real field data, each frequency provides an independent estimate of the incident and reflected spectra for any particular SNR, wave amplitude and true reflection coefficient. This allows mean values of error, and confidence intervals on these estimates, to be calculated for particular frequency ranges. By running a range of simulations with different wave amplitudes and noise levels, errors and

1 corresponding confidence intervals can be predicted for each frequency bin in a measured
 2 spectrum.
 3
 4
 5
 6

7 Synthetic time series were generated with 4096 data points and a sampling frequency of 4 Hz.
 8
 9 Smooth spectral estimates were computed using a 50% overlapping Hanning window, giving
 10 a frequency resolution of 0.0039 Hz and 12 degrees of freedom (Nutall, 1971). The spectra
 11
 12 are then separated into incident S_i and reflected S_r components using the first order formulae
 13
 14
 15
 16 of Gaillard et al. (1980) as
 17
 18
 19
 20
 21

$$22 \quad S_i(f) = \frac{\bar{S} - \bar{C} + \bar{Q}}{2S_a} \quad (3)$$

$$25 \quad S_r(f) = \frac{\bar{S} - \bar{C} - \bar{Q}}{2S_a} \quad (4)$$

27
 28
 29
 30 where
 31
 32
 33
 34
 35

$$36 \quad \bar{S} = S_1 + S_2 + S_3 \quad (5)$$

$$38 \quad \bar{C} = C_{21} \cos(k\Delta x_{21}) + C_{31} \cos(k\Delta x_{31}) + C_{32} \cos(k\Delta x_{32}) \quad (6)$$

$$41 \quad \bar{Q} = Q_{21} \sin(k\Delta x_{21}) + Q_{31} \sin(k\Delta x_{31}) + Q_{32} \sin(k\Delta x_{32}) \quad (7)$$

43
 44
 45 and
 46
 47
 48
 49
 50

$$51 \quad S_a = \sin(k\Delta x_{21}) + \sin(k\Delta x_{31}) + \sin(k\Delta x_{32}) \quad (8)$$

52
 53
 54
 55 where S, C and Q represent the auto-, co-, and quadrature-spectra respectively, Δx is sensor
 56 spacing, and subscript numbers denote sensor location (S) or sensor pair ($C, Q, \Delta x$). Co- and
 57
 58
 59
 60
 61
 62
 63
 64
 65

1 quadrature-spectra are calculated as the real and imaginary parts of the cross-spectrum,
2 respectively. The incident and reflected spectra are then used to estimate reflection
3
4 coefficients R by
5
6
7
8
9

$$10 \quad R(f) = \sqrt{\frac{s_r}{s_i}} \quad (9)$$

11
12
13
14
15

16 The purpose of using an array method with three wave gauges is to avoid singularities
17 occurring at a discrete number of critical frequencies. However, gauge triplets must be
18 chosen intelligently with spatial separations that mitigate the coincidence of critical
19 frequencies, otherwise these frequencies will suffer similar effects to those from using a two
20 gauge array. This paper will focus on the frequency range 0.01-0.33 Hz. The low frequency
21 cut-off of 0.01 Hz was chosen to avoid any adverse effects radiating from the singularity that
22 always occurs at 0 Hz, regardless of whether two of three wave gauges are used. The high
23 frequency cut-off of 0.33 Hz was chosen as it coincides with the upper limit of the frequency
24 range commonly used to define ‘short’ waves (e.g., Ruessink, 1998). Furthermore, wave
25 reflection from natural coastlines has been found to be negligible at higher frequencies,
26 particularly on dissipative beaches. The use of this frequency range allows for spectral
27 estimates at 82 discrete frequencies. To avoid the influence of singularities across the entire
28 frequency range of interest, three different array set-ups are used in the simulations to satisfy
29 frequency ranges 0.01-0.05 Hz, 0.05-0.20 Hz, and 0.20-0.33 Hz, respectively. The full range
30 of simulations was performed for each array set-up and spectral estimates for the
31 corresponding three frequency ranges were concatenated providing the full spectrum of
32 interest for each combination of simulation parameters.
33
34
35
36
37
38
39
40
41
42
43
44
45
46
47
48
49
50
51
52
53
54
55
56
57
58
59

60 **3. Results**

61
62
63
64
65

1 For each simulation scenario an assessment is made of the accuracy to which the incident and
2 reflected spectra, and corresponding reflection coefficients, are reproduced by the
3 decomposition method of Gaillard et al. (1980). Mean coherence between the three synthetic
4 time series is calculated to investigate the extent to which coherence can be used as a proxy
5 for SNR. By averaging the coherence between the three pairs of time series, fluctuations due
6 to standing wave nodes and antinodes are removed. Throughout this section, target values for
7 incident and reflected spectra and reflection coefficients (i.e., those fixed in the simulations)
8 are denoted by S_i , S_r , and R , respectively. Estimated values are differentiated from target
9 values by the following overbar symbol $\widehat{}$, and corrected estimates are represented by an
10 additional subscript c . Error in the estimated values is always positive and is therefore
11 referred to as a bias.
12
13
14
15
16
17
18
19
20
21
22
23
24
25
26
27
28

29 *3.1 Noise correction*

30
31
32
33
34 Fig. 1 shows \widehat{S}_i , \widehat{S}_r , coherence, and \widehat{R} for a wave amplitude of 2 m, $R = 0.3$, and four different
35 SNRs. With no noise added to the time series, \widehat{S}_i and \widehat{S}_r are estimated accurately with mean
36 values within 3% of their respective target values. \widehat{R} is also estimated with reasonable
37 accuracy with a mean value of 0.31. The absence of noise is reflected in a mean coherence
38 value of 0.98. A similar accuracy can be found across all simulations where no noise has been
39 added to the time series, thus providing confidence in the method. For $\text{SNR} = 2.5$, both \widehat{S}_i and
40 \widehat{S}_r are positively biased by 12.2% and 11.7% of S_i respectively, and mean coherence is
41 reduced to 0.72. With \widehat{S}_i and \widehat{S}_r being biased by practically the same amount, the difference
42 in magnitude between \widehat{S}_i and \widehat{S}_r is largely unchanged but becomes smaller relative to the
43 overall magnitudes, thus introducing a positive bias to \widehat{R} which has a mean value of 0.43.
44
45
46
47
48
49
50
51
52
53
54
55
56
57
58
59
60 This is further demonstrated by a SNR of 1.7, which creates a bias in \widehat{S}_i and \widehat{S}_r of 25.8% and
61
62
63
64
65

1 26.3% of the S_i magnitude respectively and increases the mean \hat{R} value to 0.50. A SNR of 0.7
 2 causes \hat{S}_i and \hat{S}_r to be biased by 137.4% and 136.0% of S_i respectively which raises the mean
 3 \hat{R} from 0.3 to 0.78. However, this is somewhat of an extreme case and coherence values for
 4 this simulation are below the 95% confidence threshold and therefore would not be
 5 considered significant if found in real data.
 6
 7
 8
 9

10 Whilst the bias in \hat{S}_i and \hat{S}_r is dependant only on the wave amplitude and SNR, the bias in \hat{R}
 11 becomes more significant for lower values of true reflection. This is because, while \hat{S}_i and \hat{S}_r
 12 are biased by the same amount, as the true reflection coefficient decreases from 1 the bias
 13 becomes increasingly larger relative to S_r than S_i . For a given SNR, the bias in \hat{S}_i and \hat{S}_r
 14 increases linearly with increasing wave amplitude. Therefore, normalising by \hat{S}_i conveniently
 15 removes the dependency of bias on wave amplitude, allowing the bias from all simulations to
 16 be investigated simultaneously as a function of coherence. This is shown in Fig. 2 where the
 17 data have been band-averaged across frequencies thus providing one estimate for each
 18 simulation scenario. The frequency smoothing, which increases the degrees of freedom of the
 19 estimates from 12 to 984, is performed to provide the best possible estimates from which to
 20 predict the expected bias in real data.
 21
 22
 23
 24
 25
 26
 27
 28
 29
 30
 31
 32
 33
 34
 35
 36
 37
 38
 39
 40
 41
 42
 43
 44
 45
 46
 47
 48
 49
 50
 51
 52
 53
 54
 55
 56

57 The normalised bias $\tilde{\epsilon}$ is shown to decrease exponentially with increasing coherence and an
 58 exponential regression function is fit to the data with excellent agreement and a correlation
 59 coefficient r^2 of 0.99 (all r^2 values reported herein are significant at the 95% level). This
 60 function allows for a prediction of the bias $\hat{\epsilon}$ by
 61
 62
 63
 64
 65

$$\hat{\epsilon} = \hat{S}_i 1.364 \exp(-3.705C) \quad (10)$$

1 where C is coherence. Corrected incident $\widehat{S}_{l,c}$ and reflected $\widehat{S}_{r,c}$ spectra can then be calculated

2
3 as

4
5
6
7
$$\widehat{S}_{l,c} = \widehat{S}_l - \hat{\epsilon} \tag{11}$$

8
9
10
$$\widehat{S}_{r,c} = \widehat{S}_r - \hat{\epsilon} \tag{12}$$

11
12
13
14
15 and corrected reflection coefficients \widehat{R}_c as

16
17
18
19
20
$$\widehat{R}_c = \sqrt{\frac{\widehat{S}_{r,c}}{\widehat{S}_{l,c}}} \tag{13}$$

21
22
23
24
25
26

3.2 Confidence intervals

27
28
29
30
31 Reducing the amount of frequency smoothing and degrees of freedom shown in Fig. 2
32
33 increases the amount of scatter around the exponential regression function, yet no frequency
34
35 smoothing and 12 degrees of freedom still yields an r^2 of 0.93. Regardless of the level of
36
37 frequency smoothing, values of $\tilde{\epsilon}$ remain normally distributed (according to the Shapiro-Wilk
38
39 normality test) around the exponential regression function. This allows 95% confidence
40
41 intervals on $\tilde{\epsilon}$ to be calculated for different levels of coherence and degrees of freedom using
42
43 the t-distribution. These are shown in Fig. 3a for coherence bins of 0.1 and degrees of
44
45 freedom between 12 and 984 as a result of averaging over particular frequency ranges in the
46
47 spectrum. Confidence intervals are shown to increase with decreasing coherence and the rate
48
49 of this increase is steeper for lower degrees of freedom. For example, for 12 degrees of
50
51 freedom, 95% confidence intervals are ± 0.085 and ± 0.026 for coherence values between 0.5
52
53 and 0.6, and 0.9 and 1.0, respectively. Whereas the same confidence intervals for 120 degrees
54
55
56
57
58
59
60
61
62
63
64
65

of freedom (equivalent to averaging over the infragravity band) are ± 0.037 and ± 0.010 , respectively. Note that confidence intervals are not calculated for coherence bins that include values below the 95% confidence threshold for the respective degrees of freedom. The rate of change in the confidence intervals with coherence is relatively constant and linear regression models yield r^2 between 0.81 and 0.99 for the different degrees of freedom. Figs. 3b and 3c show that the slope m and intercept b from the linear regressions can be predicted accurately ($r^2 = 0.97$ and 0.98 , respectively) using exponential regression functions and the degrees of freedom. This allows 95% confidence intervals on corrected spectra $\Delta\widehat{S}_c$ to be calculated as

$$\Delta\widehat{S}_c = \widehat{S}_l \left((-0.141 \exp(-v/69.699) - 0.015)C + (0.155 \exp(-v/67.014) + 0.022) \right) \quad (14)$$

where v is degrees of freedom. Using the standard propagation of errors, $\Delta\widehat{S}_c$ is used to calculate 95% confidence intervals on estimated reflection coefficients $\Delta\widehat{R}_c$ as

$$\Delta\widehat{R}_c = \widehat{R}_c 0.5 \left(\sqrt{\left(\frac{\Delta\widehat{S}_c}{\widehat{S}_{r,c}}\right)^2 + \left(\frac{\Delta\widehat{S}_c}{\widehat{S}_{l,c}}\right)^2} \right) \quad (15)$$

3.3 Application to simulated data

The correction technique outlined in Eqs. (10)-(15) is demonstrated in Fig. 4 on simulated data with an incident wave amplitude of 3 m and $R = 0.5$. For clarity, only incident spectra are shown in Fig. 4a-c. The same bias correction is applied to \widehat{S}_r but percentage deviations of $\widehat{S}_{r,c}$ from the target value are determined by R . With a SNR of 5.0, \widehat{S}_l is overestimated by an average of 6.56%, whereas the mean absolute error on $\widehat{S}_{l,c}$ is 1.78%. \widehat{R}_c is 0.49 which is an

1 improvement on the \widehat{R} estimate of 0.54. Corrected values are similarly accurate for a SNR of
2
3 2.5 with a mean error on $\widehat{S}_{l,c}$ of 1.83%, compared to 16.11% on \widehat{S}_l , and a mean \widehat{R}_c 0.50. A
4
5 SNR of 1.7 causes \widehat{S}_l to be overestimated by 31.66%, whilst $\widehat{S}_{l,c}$ has a mean error of 2.44%; a
6
7 decrease in error magnitude of $> 90\%$. Table 1 gives a summary of the errors and 95%
8
9 confidence intervals depicted in Fig. 4, and for additional SNRs.
10
11
12
13
14

15 SNRs less than 1 (not shown) produce biases of $> 100\%$ in \widehat{S}_l , but the accuracy of the
16
17 correction technique for these simulations remains in a reasonable range, typically less than
18
19 15%, albeit with larger confidence intervals. However, for SNRs less than ~ 1.5 , coherence
20
21 falls below the 95% confidence threshold for 12 degrees of freedom. Nevertheless, degrees of
22
23 freedom can be increased by frequency smoothing and/or increasing the number of segments
24
25 when calculating the spectra, which would reduce the 95% confidence threshold for
26
27 coherence. Therefore, it is beneficial to know that the correction technique is robust at
28
29 withstanding extreme levels of noise.
30
31
32
33
34
35
36
37
38
39
40
41
42
43
44
45
46
47
48
49
50
51
52
53
54
55
56
57
58
59
60
61
62
63
64
65

Table 1. Summary of mean errors in estimated and corrected incident spectra and reflection coefficients for a wave amplitude of 3 m, known reflection coefficient of 0.5, and SNRs between infinity and 1. Errors in the estimated and corrected incident spectra, and 95% confidence intervals on corrected incident spectra, are given in terms of percentage of the target value S_i .

SNR	\bar{C}	$\epsilon_{\widehat{S}_i}$	$\epsilon_{\widehat{S}_{i,c}}$	95% $\widehat{S}_{i,c}$	\widehat{R}	\widehat{R}_c	95% \widehat{R}_c
		%	%	%			
Inf	0.94	3.52	2.06	± 2.27	0.50	0.47	± 0.03
10.0	0.92	4.41	1.93	± 2.61	0.51	0.47	± 0.03
5.0	0.85	6.56	1.78	± 3.64	0.54	0.49	± 0.04
3.3	0.76	10.52	1.48	± 5.14	0.55	0.49	± 0.05
2.5	0.66	16.11	1.83	± 6.91	0.58	0.50	± 0.07
2	0.56	22.67	2.41	± 8.75	0.61	0.50	± 0.09
1.7	0.49	31.66	2.44	± 10.72	0.65	0.50	± 0.11
1.43	0.42	43.06	3.40	± 12.86	0.68	0.49	± 0.13
1.25	0.37	53.32	3.94	± 14.89	0.71	0.49	± 0.16
1.11	0.33	67.93	4.91	± 17.24	0.74	0.48	± 0.19
1	0.29	82.30	6.03	± 19.62	0.76	0.46	± 0.23

SNR = signal-to-noise ratio, \bar{C} = mean coherence, $\epsilon_{\widehat{S}_i}$ = mean percentage error on the estimated incident spectra, $\epsilon_{\widehat{S}_{i,c}}$ = mean percentage error on the corrected incident spectra, 95% $\widehat{S}_{i,c}$ = mean 95% confidence intervals on corrected incident spectra, \widehat{R} = mean estimated reflection coefficient, \widehat{R}_c = mean corrected reflection coefficient, 95% \widehat{R}_c = mean 95% confidence intervals on corrected reflection coefficients.

3.4 Wave angle and directional spreading

1
2 The main assumption of array methods for calculating wave reflection is that waves are
3
4 unidirectional and shore-normal. Additional numerical simulations using oblique waves
5
6 reveal that the Gaillard et al. (1980) method, and consequently the noise correction, is fairly
7
8 robust to wave angle with additional errors occurring only when the wave angle exceeds $\sim 40^\circ$
9
10 relative to shore-normal and only becoming significant ($> 10\%$) for angles exceeding $\sim 60^\circ$.
11
12 Nevertheless, these additional errors can be reduced slightly if the Gaillard et al. (1980)
13
14 method is modified to account for wave refraction effects when applied to field data.
15
16
17
18
19
20
21

22 The consequence of directionally spread waves is that the mean coherence between the
23
24 sensors will decrease without the presence of noise. This could result in an unnecessary
25
26 correction being applied to the incident and reflected spectra. For this to be significant, the
27
28 majority of wave energy would need to pass through the array at a highly oblique angle ($>$
29
30 60°). This is unlikely for data collected close to shore or in the study of infragravity waves
31
32 due to their strong refraction properties. However, one should be aware of the potential
33
34 consequences of directionally spread waves when applying the noise correction to field data
35
36 and ensure that the sensor array is aligned as close to the dominant wave direction as possible.
37
38
39
40
41
42
43

44 **4. Application to field data**

45
46 To illustrate the application of the results to field data, measurements are used from
47
48 Perranporth Beach, Cornwall, UK. Perranporth is a macrotidal, dissipative beach composed
49
50 of medium sand and exposed to both Atlantic swell and locally generated wind-sea. Data
51
52 were collected during a field experiment in November 2014 using a cross-shore array of 15
53
54 pressure transducers logging at 4 Hz. The pressure data were converted to water surface
55
56 elevation with a depth correction using linear wave theory. Spectra were calculated as with
57
58
59
60
61
62
63
64
65

1 the simulated data outlined in section 2 and separated into incident and reflected components
2 using the Gaillard et al. (1980) array method with modifications for wave shoaling analogous
3 to those implemented by Baldock and Simmonds (1999). The data presented here were
4 collected in the inner surf zone (mean water depth $\bar{h} = 1.5$ m) during a single tide with an
5 offshore significant wave height H_o of 1.85 m and a spectral peak period T_p of 10.8 s. The
6 focus of the field study was infragravity (0.005-0.05 Hz) waves and so the array set-up was
7 optimised (avoiding singularities) for estimating wave reflection in this frequency range.
8 Therefore, only infragravity data are presented here with a low frequency cut-off of 0.01 Hz
9 as with the simulated data. The analysis of co-located pressure and velocity data from a rig
10 deployed during the field experiment shows that water motion at infragravity frequencies was
11 predominantly cross-shore.
12
13
14
15
16
17
18
19
20
21
22
23
24
25
26
27
28
29
30

31 The general trend shown in Fig. 5a is of higher magnitudes of \widehat{S}_i and \widehat{S}_r at lower frequencies
32 than higher frequencies with a spectral peak at $f = 0.016$ Hz; a trend which is preserved in
33 $\widehat{S}_{i,c}$ and $\widehat{S}_{r,c}$. The largest correction in terms of spectral density occurs at the spectral peak
34 where $\widehat{S}_{i,c}$ and $\widehat{S}_{r,c}$ are reduced by 17.5% and 36.2% of \widehat{S}_i and \widehat{S}_r , respectively. Larger
35 magnitudes of both $\widehat{S}_{i,c}$ and $\widehat{S}_{r,c}$ in the low frequency portion of the infragravity band yield
36 higher \widehat{R}_c estimates with smaller corrections and confidence intervals than higher frequencies.
37 For example, at $f = 0.020$ Hz, \widehat{R}_c is 0.67 (± 0.06) which is only 0.06 less than \widehat{R} . In contrast,
38 at $f = 0.043$ Hz, the \widehat{R}_c value of 0.25 (± 0.15) is significantly less than the \widehat{R} estimate of 0.43.
39 The mean infragravity \widehat{R} is 0.61 but this is reduced in \widehat{R}_c to 0.54 (± 0.02). Whilst it isn't
40 strictly appropriate to average over the infragravity band given the frequency dependence
41 shown in the data, it does demonstrate the reduction in confidence intervals as a result of
42 more degrees of freedom.
43
44
45
46
47
48
49
50
51
52
53
54
55
56
57
58
59
60
61
62
63
64
65

1 The frequency dependence of infragravity wave reflection, with high levels of reflection
2 limited to low frequencies, is well-documented in the literature (e.g., De Bakker et al., 2014;
3 Guedes et al., 2013). The results presented here suggest that, in failing to correct for bias, \hat{R}
4 values at high infragravity frequencies where wave reflection is low, and indeed at short
5 wave frequencies where reflection tends to be even more minimal, can be overestimated by
6 more than 50%. This is likely to have impacted wave reflection estimates reported previously
7 in the literature where wave gauge arrays have been used.
8
9
10
11
12
13
14
15
16
17
18

19 **5. Conclusion**

20 An existing two-dimensional method for separating incident and reflected wave spectra using
21 an array of wave gauges is investigated for its sensitivity to random noise. Linear wave
22 theory is used to generate simulated time series of water surface elevation at three cross-shore
23 locations with varying wave amplitudes, known reflection coefficients, and signal-to-noise
24 ratios. Both the incident and reflected spectra are shown to be positively biased by noise and
25 in turn this causes reflection coefficients to be overestimated. The magnitude of the bias is
26 found to be dependent on wave amplitude, but not on the true reflection coefficient. Utilizing
27 the systematic change in coherence with noise, a relatively simple and easy to apply method
28 to correct for the observed bias is developed. This correction technique can be applied across
29 all frequencies and is considerably accurate with residual error on corrected incident spectra
30 estimates typically in the region of 2-3% for significant coherence levels; an improvement of
31 over 90% for low signal-to-noise ratios. Applying the correction to field data implies that
32 reflection coefficients can be overestimated by at least 50%. Consequently, if accurate
33 estimates of incident and reflected spectra and corresponding reflection coefficients are
34 required, then potential signal noise must be acknowledged and accounted for.
35
36
37
38
39
40
41
42
43
44
45
46
47
48
49
50
51
52
53
54
55
56
57
58
59
60
61
62
63
64
65

Acknowledgements

The authors would like to thank Sam Prodger, Kit Stokes, Tim Poate, Erwin Bergsma, Olivier Burvingt, and Peter Ganderton for their assistance during the Perranporth field experiment.

The comments and suggestions made by two reviewers helped improved the clarity of the manuscript.

References

Baldock, T.E., Simmonds, D.J., 1999. Separation of incident and reflected waves over sloping bathymetry. *Coast. Eng.* 38, 167-176. [doi:10.1016/S0378-3839\(99\)00046-0](https://doi.org/10.1016/S0378-3839(99)00046-0)

Battjes, J.A., Bakkenes, H.J., Janssen, T.T., van Dongeren, A.R., 2004. Shoaling of subharmonic gravity waves. *J. Geophys. Res.* 109, C02009.

<http://dx.doi.org/10.1029/2003JC001863>

De Bakker, A.T.M., Tissier, M.F.S., Ruessink, B.G., 2014. Shoreline dissipation of infragravity waves. *Cont. Shelf Res.* 72, 73-82. [doi:10.1016/j.csr.2013.11.013](https://doi.org/10.1016/j.csr.2013.11.013)

Frigaard, P., Brorsen, M., 1995. A time-domain method for separating incident and reflected irregular waves. *Coast. Eng.* 24, 205-215. [doi:10.1016/0378-3839\(94\)00035-V](https://doi.org/10.1016/0378-3839(94)00035-V)

Gaillard, P., Gauthier, M., Holly, F., 1980. Method of analysis of random wave experiments with reflecting coastal structures. *Proceedings of the 17th Conference on Coastal Engineering*. ASCE, New York.

1 Goda, Y., Suzuki, Y., 1976. Estimation of incident and reflected waves in random wave
2 experiments. Proceedings of the 15th Conference on Coastal Engineering. ASCE, New York.
3

4
5
6
7 Guedes, R.M.C., Bryan, K.R., Coco, G., 2013. Observations of wave energy fluxes and
8 swash motions on a low-sloping, dissipative beach. J. Geophys. Res. 118, 3651-3669.
9

10
11
12 [10.1002/jgrc.20267](https://doi.org/10.1002/jgrc.20267)
13

14
15
16 Guza, R.T., Bowen, A.J., 1976. Resonant interactions for waves breaking on a beach.
17 Proceedings of the 15th Conference on Coastal Engineering. ASCE, New York.
18
19

20
21
22
23
24 Hughes, S.A., 1993. Physical models and laboratory techniques in coastal engineering. World
25 Scientific, Singapore.
26
27

28
29
30
31 Huntley, D.A., Simmonds, D., Tatavarti, R., 1999. Use of collocated sensors to measure
32 coastal wave reflection. J. Waterw. Port Coast. Ocean Eng. 125, 46-52.
33
34

35
36 [http://dx.doi.org/10.1061/\(ASCE\)0733-950X\(1999\)125:1\(46\)](http://dx.doi.org/10.1061/(ASCE)0733-950X(1999)125:1(46))
37
38

39
40
41 Mansard, E.P.D., Funke, E.R., 1980. The measurement of incident and reflected spectra using
42 a least squares method. Proceedings of the 17th Conference on Coastal Engineering. ASCE,
43 New York.
44
45
46

47
48
49
50
51 Morden, D.B., Richey, E.P., Christensen, D.R., 1976. Decomposition of co-existing random
52 wave energy. Proceedings of the 15th Conference on Coastal Engineering. ASCE, New York.
53
54
55
56
57
58
59
60
61
62
63
64
65

1 Nutall, A.H., 1971. Spectral estimation by means of overlapped FFT processing of windowed
2 data. Report No. 4169. Naval Underwater Systems Center (NUSC), New London,
3 Connecticut.
4
5
6
7
8

9 Ruessink, B.G., 1998. The temporal and spatial variability of infragravity energy in a barred
10 nearshore zone. Cont. Shelf Res. 18, 585-605. [doi:10.1016/S0278-4343\(97\)00055-1](https://doi.org/10.1016/S0278-4343(97)00055-1)
11
12
13
14
15

16 Sheremet, A., Guza, R.T., Elgar, S., Herbers, T.H.C., 2002. Observations of nearshore
17 infragravity waves: Seaward and shoreward propagating components. J. Geophys. Res. 107,
18
19 3095. <http://dx.doi.org/10.1029/2001JC000970>
20
21
22
23
24

25 Shumway, R.H., Stoffer, D.S., 2000. Time Series Analysis and Its Applications. Springer,
26
27 New York.
28
29
30
31

32 Tatavarti, R.V.S.N., Huntley, D.A., Bowen, A.J., 1988. Incoming and outgoing wave
33 interactions on beaches. Proceedings of the 21st Conference on Coastal Engineering. ASCE,
34
35
36
37
38
39
40
41
42
43
44
45
46
47
48
49
50
51
52
53
54
55
56
57
58
59
60
61
62
63
64
65

Figure captions

Fig. 1. Estimated incident \widehat{S}_i and reflected \widehat{S}_r spectra (a-d), coherence (e-h), and estimated reflection coefficients \widehat{R} (i-l) for SNR = Inf, 2.5, 1.7, and 0.7 as stated on the figure. Dashed lines in a-d are the target incident S_i and reflected S_r spectra. Red dashed line in e-h is the 95% confidence threshold on coherence of 0.45 for 12 degrees of freedom (Shumway and Stoffer, 2000). Red dashed line in (i-l) is the target reflection coefficient R of 0.3. Wave amplitude is 2 m.

Fig. 2. Normalised bias $\tilde{\epsilon}$ (ϵ/\widehat{S}_i , where ϵ is bias) versus coherence for all wave amplitudes, true reflection coefficients, and SNRs. Data have been smoothed providing one estimate per simulation and 984 degrees of freedom. Solid red line is an exponential regression function with coefficients and accuracy given on the figure.

Fig. 3. (a) 95% confidence intervals on normalised bias $\Delta\tilde{\epsilon}$ for various degrees of freedom versus coherence. Solid lines are linear regression lines fit to the data of the corresponding colour. (b) Slopes m and (c) intercepts b from the linear regression lines shown in (a) versus degrees of freedom. Solid red lines in (b) and (c) are exponential regression functions with coefficients and accuracy given on the figure.

Fig. 4. (a-c) Deviation (%) of uncorrected \widehat{S}_i and corrected $\widehat{S}_{i,c}$ incident spectra from the target value S_i . Shaded areas are 95% confidence intervals on $\widehat{S}_{i,c}$. (d-f) Coherence, and (g-i) uncorrected \widehat{R} and corrected \widehat{R}_c reflection coefficients. Shaded areas are 95% confidence intervals on \widehat{R}_c . SNRs are 5.0, 2.5, and 1.7 as stated on the figure. Red dashed line in (d-f) is the 95% confidence threshold on coherence of 0.45 for 12 degrees of freedom (Shumway and

Stoffer, 2000). Red dashed line in (g-i) is the target reflection coefficient R of 0.5. Wave amplitude is 3 m.

Fig. 5. Data from the inner surf zone of Perranporth Beach, UK ($H_o = 1.85$ m, $T_p = 10.8$ s).

(a) Corrected incident $\widehat{S}_{i,c}$ and reflected $\widehat{S}_{r,c}$ spectra, and uncorrected incident \widehat{S}_i and reflected \widehat{S}_r spectra. Shaded areas are 95% confidence intervals on $\widehat{S}_{i,c}$ and $\widehat{S}_{r,c}$. (b)

Coherence and (c) corrected \widehat{R}_c and uncorrected \widehat{R} estimated reflection coefficients. Shaded areas are 95% confidence intervals on \widehat{R}_c . Red dashed line in (b) is the 95% confidence threshold on coherence of 0.45 for 12 degrees of freedom (Shumway and Stoffer, 2000).

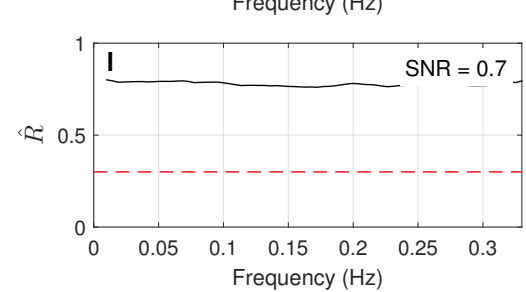
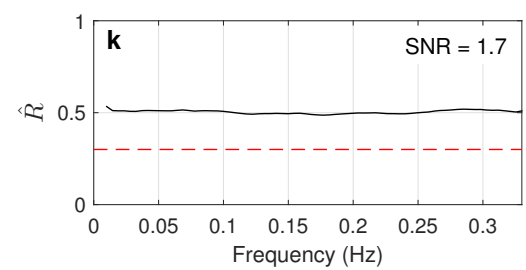
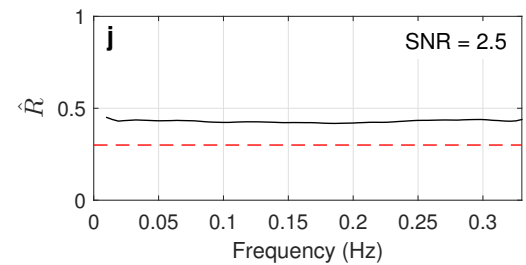
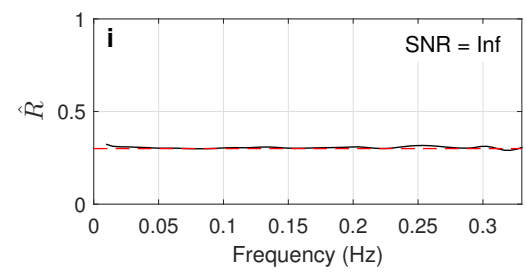
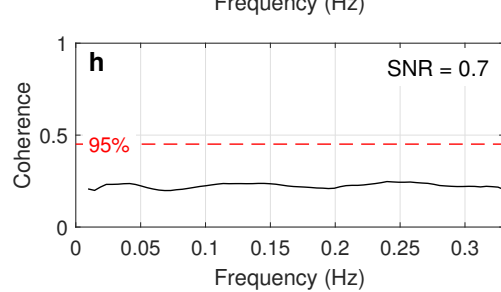
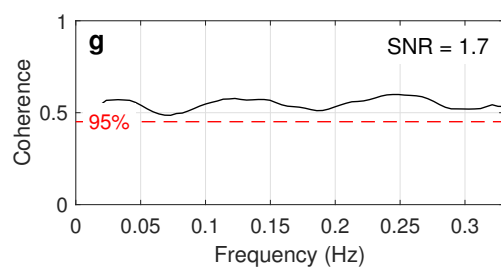
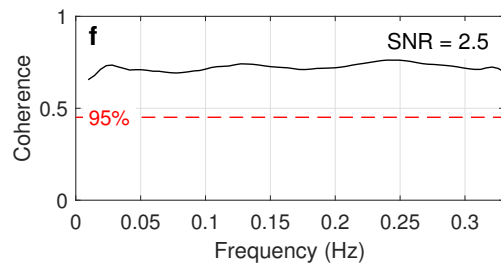
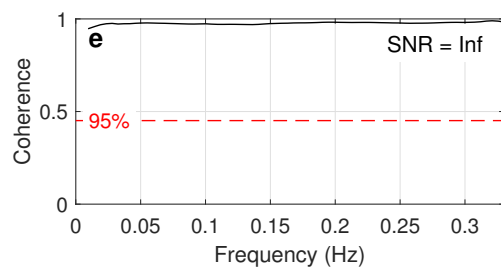
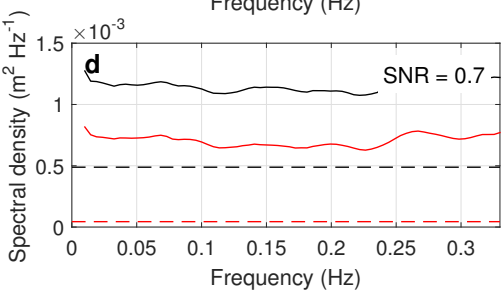
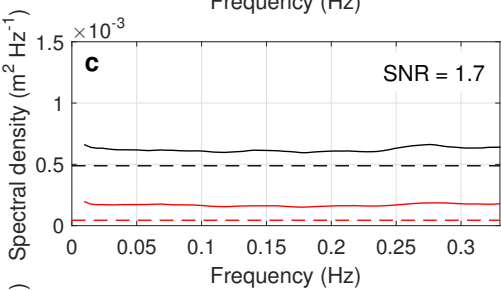
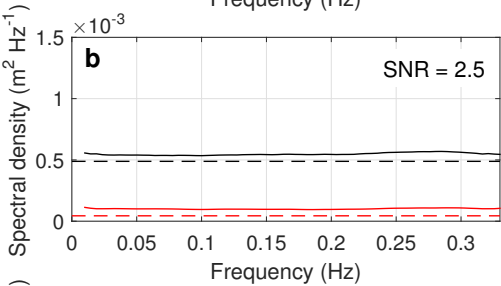
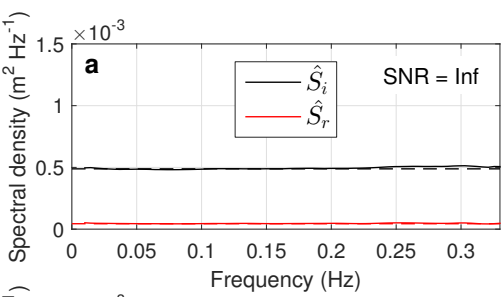
Figure 1

Figure 2

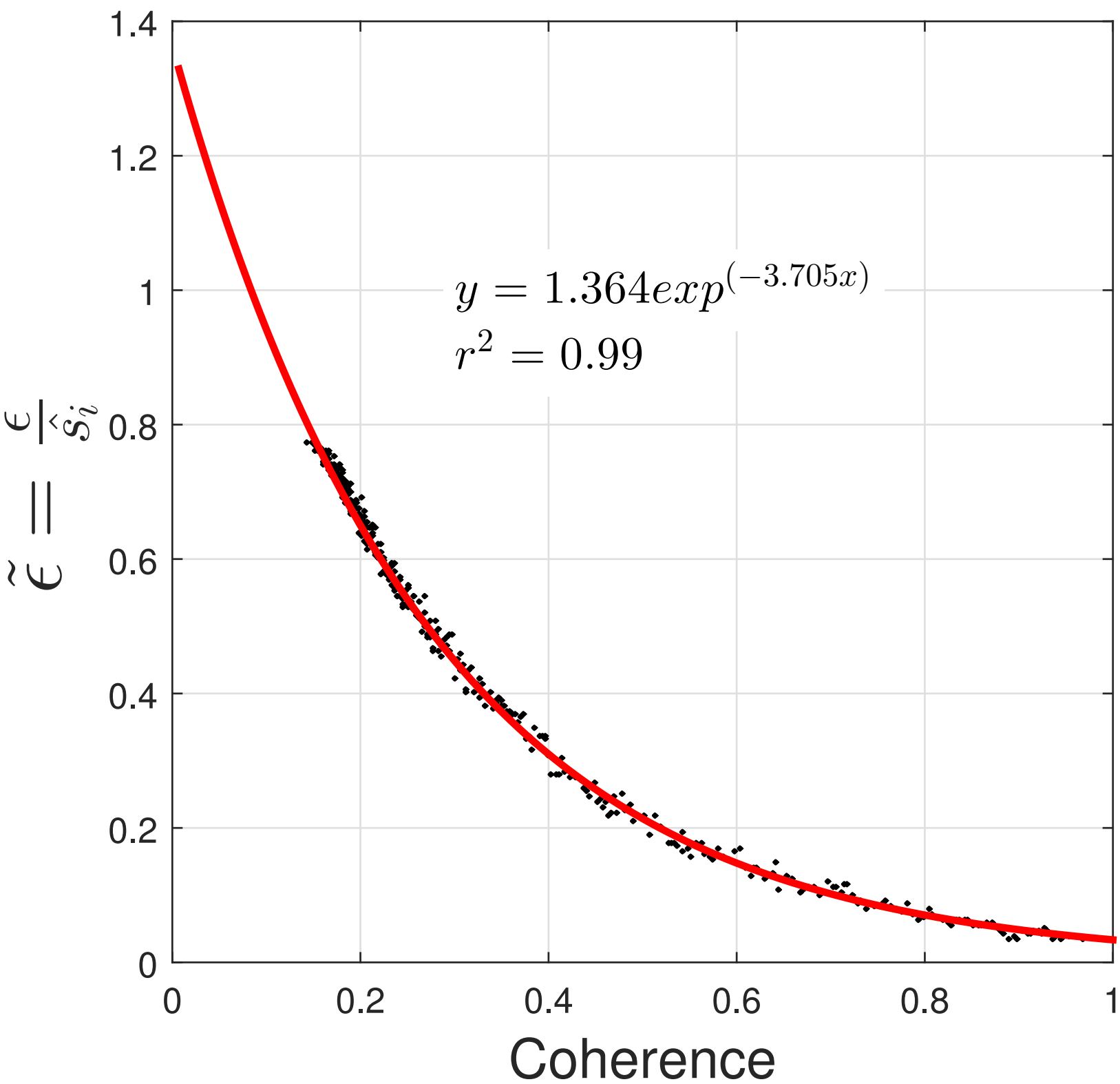


Figure 3

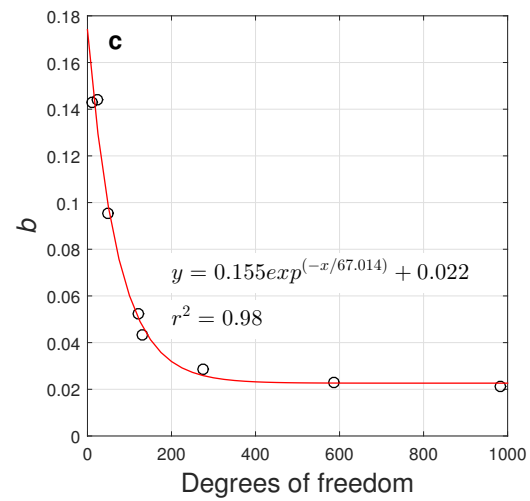
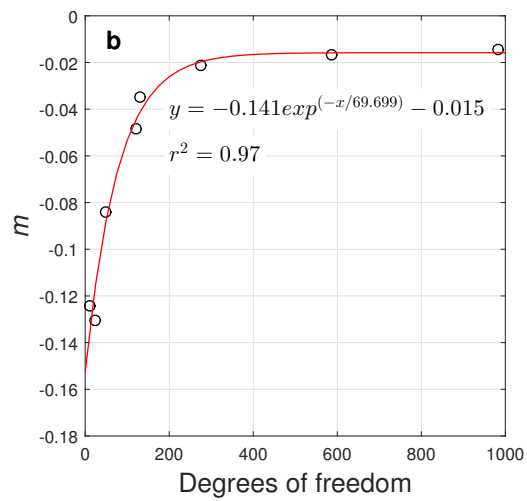
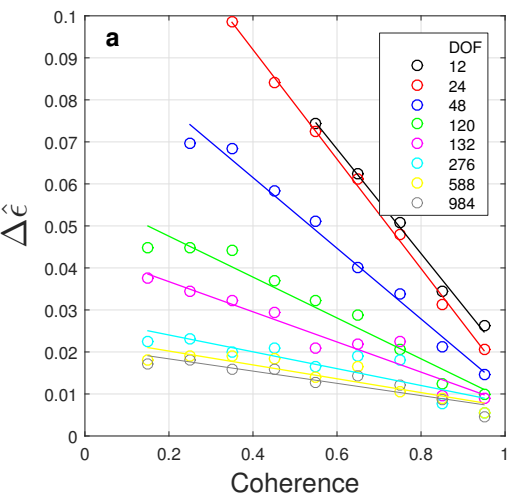


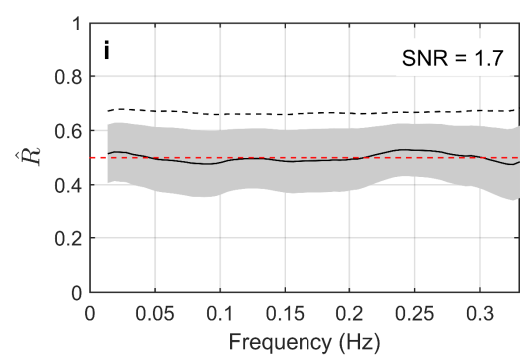
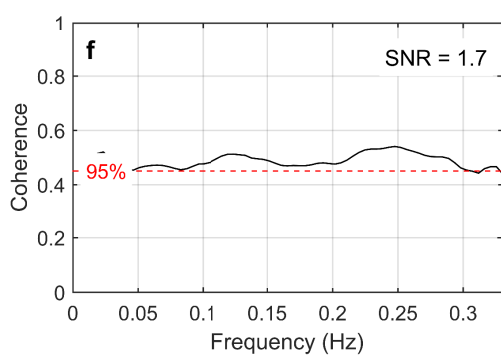
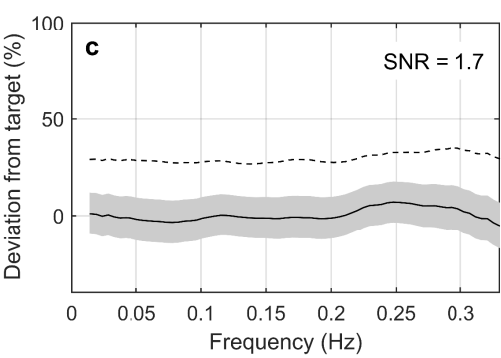
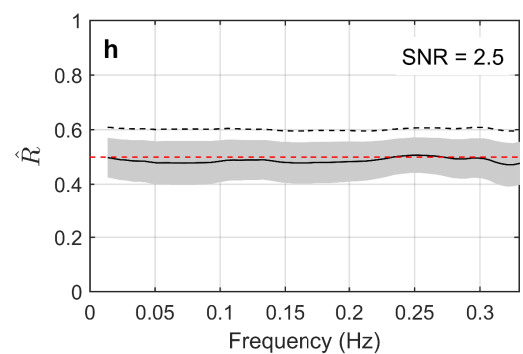
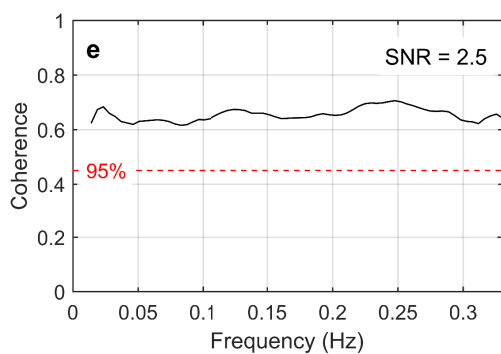
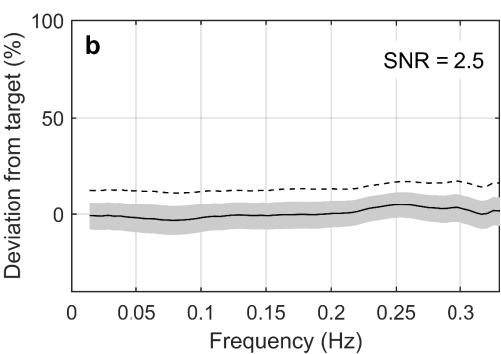
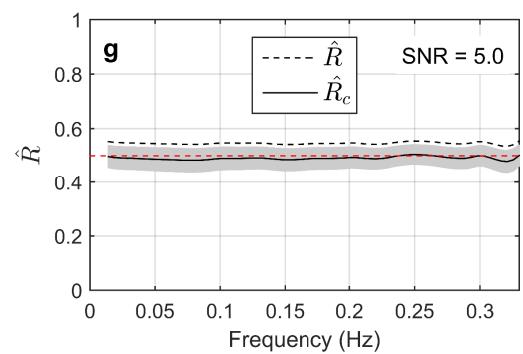
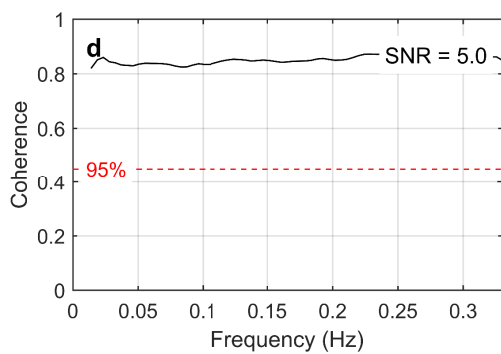
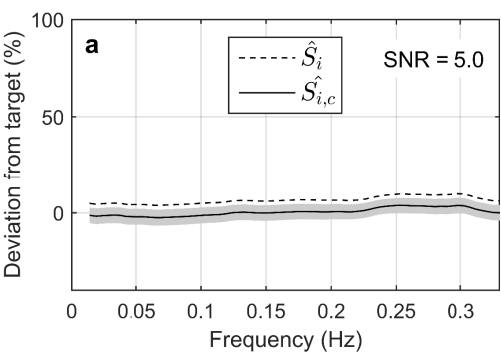
Figure 4

Figure 5

